Microfluid Nanofluid (2008) 5:631–638
DOI 10.1007/s10404-008-0281-9

RESEARCH PAPER

Formation of ionic depletion/enrichment zones in a hybrid micro-/nano-channel

Kuan-Da Huang · Ruey-Jen Yang

Received: 22 January 2008 / Accepted: 9 March 2008 / Published online: 27 March 2008

Abstract This study fabricates a cross-form microchip in which the two side channels are attached to the main channel via a nanochannel bridge. Ionic depletion and enrichment zones are established on the anodic and cathodic sides of the nanochannel. Results show that the low conductivity within the depletion zone induces a rapid electroosmotic flow, which in turn prompts the generation of vortex flow structures within the depletion zone. Both the lengthening of the depletion bulk charge layer and decrease in length of the diffusion layer as the applied voltage is increased are also demonstrated in this study.

Keywords Concentration polarization · Electroosmosis · Nanofluidics · Microfluidics

1 Introduction

Developments in the nanofluidics field over the past few years possibly now make the fabrication of sophisticated microscale devices for a variety of applications, for example: energy conservation (Daiguji et al. 2004), transistor (Karnik et al. 2005), ionic rectifier (Cheng and Guo 2007) etc. In nanochannels, the channel dimension approaches the thickness of the electrical double layer (EDL) and hence an overlap of the EDL occurs, given a suitable buffer concentration. When the buffer solution and sample species are introduced into such channels, they exhibit quite different phenomena from those observed within microchannels, including a lower electroosmotic flow rate (Hunter 1981), an approximately constant surface charge density (Stein et al. 2004; Huang and Yang 2007), an ionic exclusion–enrichment effect (EEE) (Pu et al. 2004; Plecis et al. 2005), and so forth. In the EEE phenomenon, the counter-ion enrichment and co-ion exclusion effects are the result of electrostatic interactions between the species and the charged nanochannel surface. The perm-selectivity effect induced by the EEE phenomenon was first investigated experimentally in the context of nanoporous membranes. This results in a concentration gradient near the entrance and exit of the nanochannel, which is called concentration polarization (Probstein 1994).

In earlier studies, the concentration polarization led to a specific issue about the limiting current and over-limiting current when an electric field is applied across a perm-selectivity membrane. Rubinstein and Shtilman (1979) studied the voltage against current curves of cation exchange membranes and recognized that the current is mainly transferred across the membrane by salt cations. Dukhin and Mishchuk (1993) applied the effect of the over-limiting current to intensify the electrodialysis. Pu et al. (2004) fabricated eight parallel 60-nm-deep nanochannels and found that both positively and negatively charged ions were enriched at the cathodic end of the nanochannel, while the depletion region occurred at the anodic end. The authors referred to this phenomenon as the ion-enrichment and ion-depletion effect. The same phenomenon was also observed in an earlier study by Kuo et al. (2003) in a hybrid channel incorporating two microchannels and a polycarbonate nuclear track-etched (PCTE) membrane. Kim et al. (2007) correlated a relation for concentration polarization and the limiting current

Electronic supplementary material The online version of this article (doi:10.1007/s10404-008-0281-9) contains supplementary material, which is available to authorized users.

K.-D. Huang · R.-J. Yang (✉)
Department of Engineering Science,
National Cheng Kung University, Tainan 70101, Taiwan
e-mail: rjyang@mail.ncku.edu.tw

behavior. Therefore, the ion-enrichment effect in nanochannels can be well-associated with the over-limiting current in exchange membranes (Rubinstein and Shtilman 1979).

In addition, the ion-depletion effect accompanied the ion-enrichment effect at the other end of the nanochannel also associated a specific phenomenon, which is named as bulk charged layer (secondary double layer). Rubinstein et al. (1979) explained the development of bulk charge region by the concept of a rejection of the electroneutrality condition near the exchange membrane. Dukhin's (1991) effort in investigating the electrokinetic phenomena induced by bulk charge (second kind) is different from that induced by surface charge (first kind), and the bulk charge layer (i.e. secondary double layer) is the major manifestation of electroosmosis of the second kind. The bulk charge layer due to the electroosmosis of the second kind (Dukhin 1991) will result in a high electric field in the vicinity of the exchange membrane. This layer creates a low-conductivity region which induces a rapid electroosmotic flow near the membrane. Ben and Chang (2002) applied the theory of the second kind to analyze the potential distribution and the tangential electrical field on an ion-selective porous granule. Dukhin (1991) observed the vortices near the curved granule surface, and Takhistov et al. (2003) found the formation of vortices near the microchannel junctions. To maintain the total flow balance, a pressure gradient is established to reduce the overall flow rate in this high velocity region. The combined effects of the pressure-driven flow and the electroosmotic flow result in the formation of vortices in the bulk charge layer (Takhistov et al. 2003). Recently, Kim et al. (2007) utilized a nanochannel array as an exchange membrane to generate a bulk charged region in microchannels and observed the similar recirculation structures.

The current study performs an experimental and numerical investigation into the formation of ionic depletion and enrichment zones in a nanochannel under the effect of an applied electrical field. Using conventional photolithography and wet chemical etching processes, a cross-form microchip is fabricated in which the two side channels are connected to the main channel via a nanochannel bridge. It is shown experimentally that the application of an electrical field to the microchip creates an ionic depletion effect in the anodic side of the nanochannel and an ionic enrichment effect in the cathodic side. The size of the depletion zone depending on the applied electrical field is investigated. Numerical simulations indicate that the reduction in local conductivity in the ionic depletion region leads to the formation of high-speed recirculations in the bulk charge layer. The existence of these recirculations is demonstrated experimentally by injecting latex particles into the buffer solution.

2 Methodologies

Figure 1a presents a schematic illustration and an experimental image of the proposed cross-form microchip. The device was fabricated on sodium-glass substrates using standard photolithography techniques [positive photoresist (AZ4620), a photomask and a UV exposure process (G-line)]. The exposed substrates were etched in buffered oxide etchant (BOE, 7:1) without agitation at room temperature. The upper and lower substrates were then aligned under a microscope and pre-bonded using DI water. Finally, a permanent joint was formed between the two plates using a fusion bonding process (Pan et al. 2006).

As shown in Fig. 1b, the microchip incorporates two major components, namely a lower plate containing the main channel and the two side channels, respectively, and an upper plate containing the nanochannel. The main channel and two side channels have a width of 100 μm, a depth of 25 μm and lengths of 20 and 10 mm, respectively.

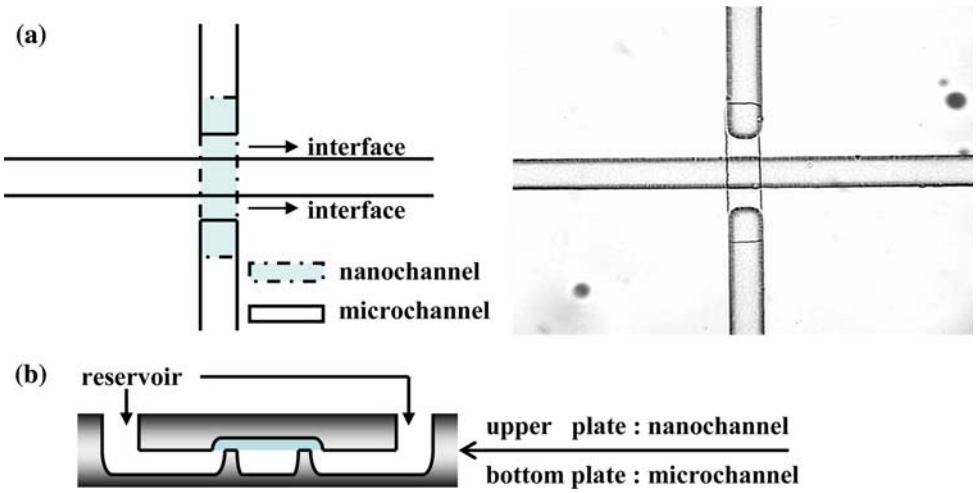

Fig. 1 Cross-form microchip: **a** schematic illustration of microchannels and nanochannel and photograph of bonded microfluidic device fabricated on glass substrate, **b** schematic illustration of cross-section of microchip showing major channel, side channels and nanochannel. The microchannels have a width of 100 μm, a depth of 25 μm and lengths of 20 and 10 mm, respectively. The gap between the major channel and the two side channels is 80 μm. The nanochannel has a depth about 100 nm

The gap between the main channel and the two side channels is 80 μm. The nanochannel has a depth about 100 nm. Overall, the microchip measures 4 cm × 4 cm.

During the experiments, the channels and reservoirs of the microchip were filled with a buffer solution (sodium tetraborate-10-hydrate, pH = 9.2, Aldrich) and positively charged Rhodamine 6G (R6G) fluorescent dye. The buffer/sample solution was driven electrokinetically by applying a DC voltage to the microchip reservoirs. The R6G species was observed using a mercury-lamp-induced fluorescence technique. The experimental images were captured by an optical microscope (Eclipse 50I, Nikon, Japan) fitted with a 4× magnification objective lens (numerical aperture = 0.13). The images were then coupled into a charge-coupled device (CCD) camera (SSC-DC50A, Sony, Japan) operated in video mode at an acquisition rate of 30 images per second. The fluorescence intensity over the range 10^{-2} M to 10^{-6} M was identified using ND4, ND8 and ND16 filters, respectively. The variation of conductivity within the depletion region can be estimated by DC measurements (Keithley 2400 source/measure unit). The flow structures established in the vicinity of the microchannel/nanochannel intersection were visualized by introducing 2-μm diameter polystyrene particles (Polysciences Inc., Warrington, PA, USA) into the buffer.

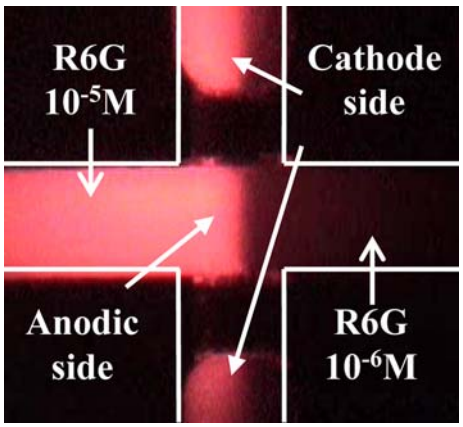

Fig. 2 The charged species with 10^{-2} M buffer solution and 10^{-5} M/10^{-6} M R6G pass through the nanochannel over the course of 60 s (EDL thickness is about 3 nm, non-overlapped)

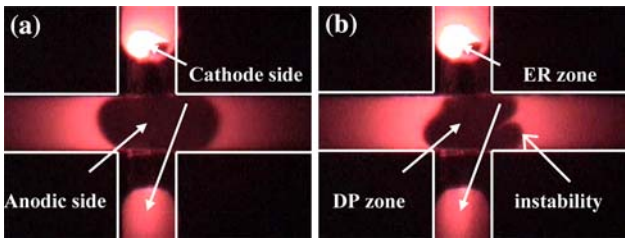

Fig. 3 10^{-5} M R6G transport through microchip with 10^{-3} M buffer solution and driving voltage of 400 V: **a** simultaneous formation of depletion zone in anodic side and enrichment effect in cathodic side, **b** concentration boundary disturbed by EKI effect

3 Results and discussions

3.1 Depletion–enrichment effect

Figure 2 presents experimental images of the species transport through the nanochannel over the course of 60 s. In this example, 10^{-5} M R6G is introduced from the left side of the main channel, whereas 10^{-6} M R6G is added from the right side. The samples are driven through the microchip by applying a voltage of 400 V DC to the left and right reservoirs of the microchip, respectively, while grounding the two side channels. In this example, the R6G species are mixed with a 10^{-2} M buffer solution. According to the Gouy–Chapmann model (Hunter 1981), the EDL thickness (λ_d) is approximately 3 nm for an electrolyte of this concentration. This thickness is insufficient to result in an overlapped EDL condition at the interface between the main channel and the nanochannel. As a result, the interface between the two samples streams in the nanochannel and side channel regions of the microchip has a smooth and well-defined appearance, as shown in Fig. 2.

A second experiment was performed in which the channels are again filled with 10^{-5} M R6G species and a 10^{-3} M buffer solution, as shown in Fig. 3. As before, a DC voltage of 400 V was applied at both ends of the main channel, while the two side channels were grounded. Due to the weaker concentration of the buffer solution used in this experiment, the thickness of the EDL (λ_d) increases to approximately 10 nm, and thus some overlap effects can be expected with EDL thickness of 10 nm in a 100 nm channel. Note that EDL thickness parameter (h/λ_d) provides only a characteristic length scale of the EDL which actually has a slow decay because the thickness of the EDL increases inversely as the square root of the buffer concentration, $\lambda_d \sim c^{-1/2}$. Since the dimensions of the nanochannel ($\sim$100 nm) are close to the magnitude of the EDL thickness, an excessive positive ionic flux enters the nanochannel and forms a discernible ionic enrichment (ER) zone at the cathodic end and an ionic depletion zone (DP zone) at the anodic end, as shown in Fig. 3a. However, the DP zone has a lower conductivity than the other regions in the main channel, and hence an electrokinetic instability (EKI) effect (Chen et al. 2005) is induced. As shown in Fig. 3b, the EKI effect disturbs the concentration boundary but does not prevent the final formation of a DP zone in the intersection region of the microchip. The enrichment effect exhibited more pronounced resulting in an increase of the R6G fluorescence intensity from 10^{-5} M to $\sim 10^{-3}$ M (see the animation in the Supporting Information). As noted earlier, a similar phenomenon also occurs in the lower region of the

microchip intersection region, but is less pronounced (and therefore less easily detected). The possible reason could be ascribed to a height difference between the two nanochannels. Figure 4 shows the evolution of the ER zone within the microchip when the voltage configuration is reversed by switching the cathode from the side channel reservoir to the end of the main channel (Fig. 4a, d), at time $t = 3$ and 40 s, respectively (see the animation in the Supporting Information). As shown, and as time elapses, the positive ionic flux accumulated in the side channel during the previous step in which the side channel was grounded gradually migrates into the cathodic side of the nanochannel. As a result, an ER zone is created within the intersection region of the microchip (i.e. the new cathodic side of the nanochannel) and a DP zone is formed in the side channel (i.e. the new anodic side of the nanochannel).

3.2 Concentration distribution in depletion zone

In this study, we chose the R6G to observe the counter-ion behavior near the micro/nano intersection and tried to find diffusion layer and bulk charged layer in the DP zone. The experimental images presented in Fig. 2 show that an obvious R6G concentration boundary is established when the depletion effect is induced in the anodic side of the nanochannel. In other words, the DP zone corresponds to a concentration polarization region. (Note that the ionic depletion/enrichment effect applies not only to the R6G species, but also to the buffer solution. In the current experiments, a fluorescent R6G species sample is used to visualize that variation in size of this DP zone.) In this study, it is speculated that the thickness of the diffusion layer is reduced as a result of the formation of a flow field with a high Peclet (Pe) number within the DP zone. In principle, a high Pe number implies that the convection effect is stronger than the diffusion effect. In the current case, electroosmosis of the second kind generates a higher-order convection effect because the bulk charge layer has an extremely low electrical conductivity and therefore induces a high-intensity electrical field in the anodic side of the nanochannel. Thus, it can be anticipated that the thickness of the diffusion layer will reduce as the intensity of the driving field increases. By contrast, the thickness of the bulk charge layer will increase with an increasing applied voltage (or current density). Note that similar results were presented by Mishchuk (1999), who studied the concentration polarization effect in ion-exchange particles and provided the following scaling relations:

$$S_o \sim \phi^{2/3}\delta^{1/3}, \quad \delta \sim \phi^{-1/2} \tag{1}$$

where S_o is the thickness of the induced bulk charge layer, δ is the thickness of the diffusion layer, ϕ is the applied potential.

As discussed earlier, the concentration polarization region, i.e. the DP zone, is composed of three layers. Figure 5 presents a light intensity analysis along the main channel of the cross-form microchip under applied voltages of 50, 100 and 400 V, respectively. The results are acquired using ImagePro software (MediaCybernetics Inc., Silver Spring, MD, USA) and show the variations of the background, R6G (initial) and R6G (voltage-driven) intensities along the dotted center lines indicated in the three experimental images. As shown, the variations of the initial and voltage-driven R6G intensity signals enable the boundaries of the diffusion layer and bulk charge layer components of the DP zone to be identified in each case. The results confirm that the thickness of the diffusion layer decreases with increasing voltage, whereas that of the bulk charge layer increases. In addition, these results can also be seen that the light intensity of the voltage-driven R6G sample outside of the DP zone exceeds that of the original sample. This result also confirms the preconcentration effect within the main channel as a result of the conductivity difference (Wang et al. 2005).

3.3 Flow field in depletion/enrichment zone

The intensity of the electrical field distribution within the microchip varies both as a result of the abrupt change in the channel dimensions at the interface between the main channel and the nanochannel, and the concentration polarization effect. The concentration difference in the depletion region affects both the magnitude of the electrical conductivity (σ) and the zeta potential (ζ). In accordance with the principles of current continuity, the changes induced in the electrical field (E) within the microchannel as a result of this non-homogenous conductivity distribution can be expressed as

$$E \sim \sigma^{-1} \sim c^{-1}, \tag{2}$$

where c is buffer concentration. The zeta potential on the microchannel and nanochannel walls varies with the

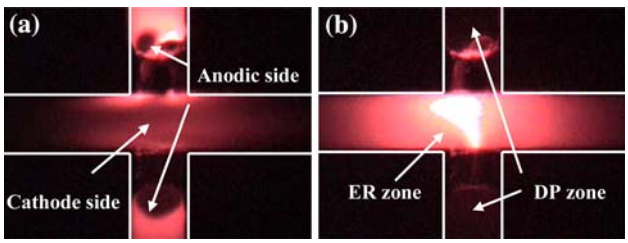

Fig. 4 Migration of collected positive ionic flux from side channel to intersection region of cross-form microchip under application of 400 V driving voltage to side channel and ground condition to main channel. **a** and **b** correspond to elapsed times of 3 s and 40 s, respectively

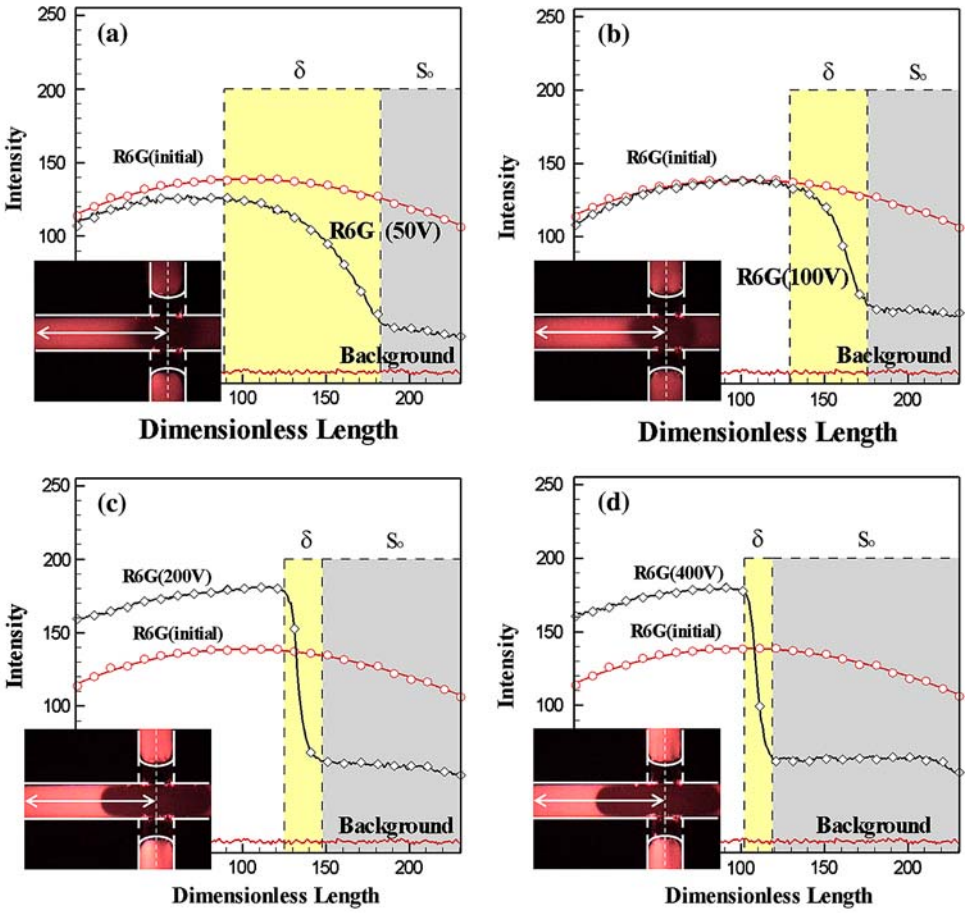

Fig. 5 Light intensity analysis in main channel showing diffusion layer and bulk charge layer within depletion zone under applied voltages of: **a** 50 V, **b** 100 V, **c** 200 V and **d** 400 V, respectively. Note that S_o is the thickness of the induced bulk charge layer, δ is the thickness of the diffusion layer

concentration in accordance with Kirby and Hasselbrink (2004)

$$\begin{aligned} &\zeta \sim c^{-1/2}, \text{ low } \zeta, \\ &\zeta \sim \log c, \text{ high } \zeta. \end{aligned} \tag{3}$$

Therefore, the concentration difference has a significant effect on the electroosmotic velocity both as a result of the changes induced in the electrical field and the variation induced in the zeta potential. However, based on a scaling analysis, the concentration polarization phenomenon induced at the junction between the microchannel and the nanochannel has a greater effect on the electrical field than on the zeta potential.

According to Eq. (2), the DP zone generates a high-intensity electrical field, whereas the ER zone results in a low-intensity electrical field. In this study, numerical simulations were performed to simulate the corresponding flow fields in the DP and ER zones in the main channel, as shown in Fig. 6 (note that a full description of the simulation procedure is presented by the current group, Chang and Yang 2004). Figure 6a presents a simplified computational domain containing the original concentration (with conductivity σ_o) region and DP/ER (with conductivity σ_c) zone. Note that the conductivity is dominated by the buffer solution. Accordingly, in performing numerical simulations, the value of the conductivity ratio, $\gamma = \sigma_c/\sigma_0$ was purposely specified in the DP and ER zones when modeling the flow fields. Here, $\gamma < 1$ and $\gamma > 1$ indicate the depletion effect and enrichment effect, respectively. Figure 6b shows the flow fields of the ER zone corresponding to Fig. 4 ($\gamma = 10$), whereas Fig. 6c presents the DP zones corresponding to Fig. 3 ($\gamma = 10$). Boundary conditions are specified as the following:

$$\begin{aligned} &\mathrm{B_m(microchannel\ in/outflow)}: \ p = 0, \ \ \mathbf{n}\cdot\nabla\mathbf{u} = 0, \\ &\phi = \Phi(\text{for DP}), \ \phi = 0\,(\text{for ER}) \end{aligned} \tag{4}$$

$$\mathrm{B_w(wall)}: \mathbf{n}\cdot\nabla p = 0, \text{slip condition(Eq.(7))}, \mathbf{n}\cdot\nabla\phi = 0 \tag{5}$$

$$\begin{aligned} &\mathrm{B_n(micro/nano\ intersection)}: \mathbf{n}\cdot\nabla p = 0, \\ &\qquad\qquad\qquad\qquad \phi = 0\,(\text{for DP}), \\ &\qquad\qquad\qquad\qquad \phi = \Phi\ (\text{for ER}) \end{aligned} \tag{6}$$

where the symbol "**n**" represents the direction normal to the boundary. The slip condition is given by the Helmholtz–Smoluchowski velocity relation, i.e.

$$\mathbf{u} = -\frac{\varepsilon\varepsilon_0\zeta}{\mu}E, \tag{7}$$

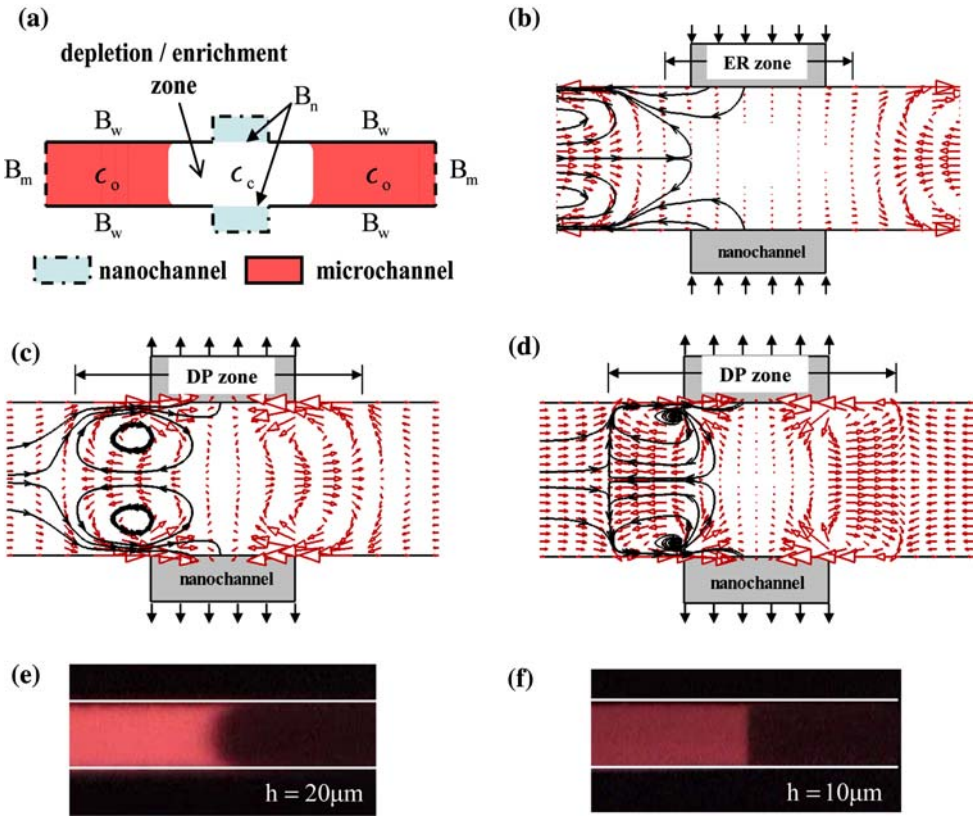

Fig. 6 Numerical results for flow fields in DP zone and ER zone in main channel: **a** schematic illustration of simplified domain in main channel; **b** and **c** flow fields corresponding to ER zone ($\gamma = 10$) and DP zone ($\gamma = 0.1$), respectively; **d** flow field in a shallower main channel corresponding to DP zone; **e** and **f** show the experimental result with channel height of 20 μm and 10 μm, respectively

where ε is the dielectric constant of water, ε_0 is the permittivity of a vacuum, and μ is the fluid viscosity. The present simulation assumes that the zeta potential $\zeta = -75$ mV according to the used buffer solution (counter-ion: Na^+ and pH = 9.2).

In the cross-form microchip developed in the current study, the velocity in the main channel is significantly higher than that in the nanochannel due to the overlapped EDL. This velocity difference results in a pressure gradient which prompts the formation of recirculation structures within the main channel in the vicinity of the intersection. To reflect the lower electroosmotic velocity (EOF) in the nanochannel, comparing to that in the microchannel, an estimated averaged-EOF was applied at the intersection of the main channel and the nanochannel. This boundary condition was based on a correction function G, defined as (Hunter 1981)

$$G(\kappa h) \approx \frac{\tan h\kappa h}{\kappa h}, \tag{8}$$

where $1/\kappa$ is the Debye screening length (λ_d), κ is given by $\kappa = \sqrt{2z_i^2 e^2 c_0/\varepsilon\varepsilon_0 kT}$, h the channel height, k the Boltzmann constant and T the local temperature. For instance, the G factor is ~ 0.924 for the condition of $kh = 1$. This value indicates that the averaged-EOF decreases 92.4% compared with that for the condition of $kh > 1{,}000$ ($G \sim 0$). However, the velocity difference at the micro/nano intersection should induce a back-pressure to satisfy the mass conservation. Here, we assume the induced pressure will not increase the flow rate in the nanochanel, but will reduce the flow rate in the microchannel. This assumption is based on the fact that the flow resistance is proportional to h^{-3}. Therefore, the velocity at the B_n is modified to $\mathbf{u}_n = (1 - G)\mathbf{u}$. In addition, the location of the DP/ER zone is identified by the observation from our experimental images.

As shown in Fig. 6b, the ER zone is a low-velocity region (low Pe number) which collects the excess ionic flux received from the nanochannel. The streamline in Fig. 6b reveals the direction of the species transported from the nanochannel to the microchannel. This simulation is in good agreement with the experimental image shown in Fig. 4. As a result of the recirculation structures, the positive ionic flux is transported along the edge of the side channel and gradually diffuses into the intersection region of the microchip, forming the ER zone. In the DP zones shown in Fig. 6c, the low conductivity region induces a high electrical field and results in the formation of recirculation structures to ensure mass conservation (Takhistov et al. 2003). However, the recirculation structures cause the convective flux to travel in an opposite direction in the center of the microchannel. The

opposing convective flux in the DP zone blocks the species transport and therefore confines the species to a region close to the side of the microchannel. In addition, the high velocity induced by the high electrical field restrains the diffusion effect (i.e. results in a higher Pe number). Therefore, meniscus-shaped concentration boundaries are formed in the DP zone in the experimental images of Fig. 6e. The recirculation forces fresh fluid to the side-edge of the main channel. It introduces this non-depleted fluid to the entrance of the nanochannel and thus there seems to be somewhat of a positive feedback effect here. Partial of this non-depleted fluid may be entrained into the vortices. In Fig. 5, comparing to the results of 50, 100, and 200 V, the depletion region presents a higher light intensity when 400 V is applied. In addition, we changed the channel depth from 20 to 10 μm in our experiments and performed the flow field calculation in DP zone by using a 3D numerical simulation, as shown in Fig. 6d. We observe the shape of the concentration boundary changing from a meniscus-shaped (Fig. 6e) to a near flat-shaped profile (Fig. 6f) due to the shallower channel depth, as a result of Hele–Shaw flow.

Finally, the recirculation structures predicted in the numerical simulations were visualized by injecting a colloidal suspension of 2-μm latex particles into the buffer solution. Note that even though these particles are charged, they still flow toward the cathode due to the electroosmotic flow. Figure 7 presents the visualized flow fields in the vicinity of the microchannel/nanochannel intersection (see the animation in the Supporting Information). Note that the images correspond to an applied voltage of 400 V DC, a 10^{-3} M buffer solution. It is apparent that the recirculation structures are consistent with those observed in Fig. 3 and predicted Fig. 6c.

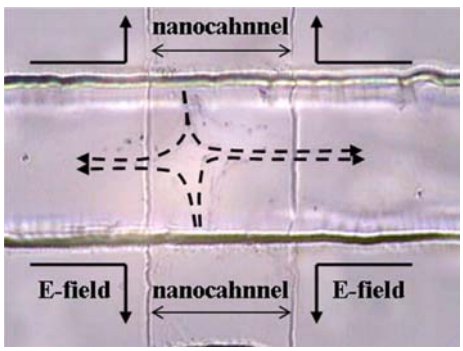

Fig. 7 Recirculation structures in DP zone. The *solid line* indicated the direction of the electrical field and the *dashed lines* indicated the particle trajectory along the bulk flow. Note flow fields are visualized using latex particles and correspond to operating conditions applied in Fig. 3

4 Conclusions

This study has fabricated a cross-form microchannel in which the two side channels are attached to the main channel by a nanochannel "bridge". The experimental results have demonstrated that the use of a buffer with an appropriate concentration results in the formation of a semi-permeable membrane at the intersection between the main channel and the nanochannel as a result of an overlapping of the electrical double layer. By introducing a positively charged fluorescent sample (R6G) into the microchip, it has been shown that an ionic depletion zone is formed in the anodic side of the nanochannel, while an ionic enrichment zone is formed in the cathodic side. The DP zone has been discussed in terms of the principles of electroosmosis of the second kind. A light intensity analysis has shown that the DP zone incorporates two distinct layers, namely the bulk charge layer and the diffusion layer. As the magnitude of the applied voltage is increased, the thickness of the bulk charge layer increases, but that of the diffusion layer reduces as a result of an increased convection effect, and thus a well-defined concentration boundary is formed. The numerical results have shown that the lower conductivity of the DP zone leads to the formation of high-speed recirculation structures to satisfy mass conservation. These structures confine the positive ionic flux to the edge of the microchannel and prompt its migration to the ER zone in the cathodic side of the nanochannel. By contrast, the ER zones are characterized by high conductivity, and the resulting low velocity flow fields results in a collection of the excess ionic flux. The flow structures predicted by the numerical results have been confirmed by injecting latex particles into the buffer solution. We also found the variation of concentration boundaries changing from a meniscus-shape to a flat-shape due to a shallower channel height. Overall, the results and discussions presented in this study provide a further understanding of the ionic depletion and enrichment effect in nanochannels.

Acknowledgments The authors gratefully acknowledge the financial support provided to this study by the National Science Council of Taiwan under Grant no. NSC-96-2628-E-006-162-MY3.

References

Ben Y, Chang HC (2002) Nonlinear Smoluchowski slip velocity and micro-vortex generation. J Fluid Mech 461:229–238

Chang C-C, Yang R-J (2004) Computational analysis of electrokinetically driven flow mixing in microchannels with patterned blocks. J Micromech Microeng 14:550–558

Chen C-H, Lin H, Lele SK, Santiago JG (2005) Convective and absolute electrokinetic instability with conductivity gradients. J Fluid Mech 524:263–303

Cheng L-J, Guo LJ (2007) Rectified ion transport through concentration gradient in homogeneous silica. Nanochannels. Nano Lett 7:3165–3171

Daiguji H, Yang P, Szeri AJ, Majumdar A (2004) Electrochemomechanical energy conversion in nanofluidic channels. Nano Lett 4:2315–2321

Dukhin SS (1991) Electrokinetic phenomena of the second kind and their applications. Adv Colloid Interface Sci 35:173–196

Dukhin SS, Mishchuk NA (1993) Intensification of electrodialysis based on electroosmosis of the second kind. J Memb Sci 79:199–210

Huang K-D, Yang R-J (2007) Electrokinetic behaviour of overlapped electric double layers in nanofluidic channels. Nanotech 18:115701

Hunter RJ (1981) Zeta potential in colloid science. Academic Press, New York

Karnik R, Fan R, Yue M, Li D, Yang P, Majumdar A (2005) Electrostatic control of ions and molecules in nanofluidic transistors. Nano Lett 5:943–948

Kim SJ, Wang Y-C, Lee JH, Jang H, Han J (2007) Concentration polarization and nonlinear electrokinetic flow near a nanofluidic channel. Phys Rev Lett 99:044501

Kirby BJ, Hasselbrink Jr EF (2004) Zeta potential of microfluidic substrates: 1. theory, experimental techniques, and effects on separations. Electrophoresis 25:187–202

Kuo TC, Cannon Jr DM, Shannon MA, Bohn PW, Sweedler JV (2003) Hybrid three-dimensional nanofluidic/microfluidic devices using molecular gates. Sens Actuators A 102:223–233

Mishchuk NA (1999) The role of water dissociation in concentration polarization of disperse particles. Colloids Surf A 159:467–475

Pan Y-J, Lin J-J, Luo W-J, Yang R-J (2006) Sample flow switching techniques on microfluidic chips. Biosens Bioelectron 21:1644–1648

Plecis A, Schoch RB, Renaud P (2005) Ionic transport phenomena in nanofluidics: experimental and theoretical study of the exclusion-enrichment effect on a chip. Nano Lett 5:1147–1155

Probstein RF (1994) Physicochemical hydrodynamics: an introduction. Wiley, New York

Pu Q, Yun J, Temkin H, Liu S (2004) Ion-enrichment and ion-depletion effect of nanochannel structures. Nano Lett 4:1099–1103

Rubinstein I, Shtilman L (1979) Voltage against current curves of cation exchange membranes. J Chem Soc Faraday Trans 75:231–246

Stein D, Kruithof M, Dekker C (2004) Surface-charge-governed ion transport in nanofluidic channels. Phys Rev Lett 93:035901

Takhistov P, Duginova K, Chang HC (2003) Electrokinetic mixing vortices due to electrolyte depletion at microchannel junctions. J Colloid Interface Sci 263:133–143

Wang Y-C, Stevens AL, Han J (2005) Million-fold preconcentration of proteins and peptides by nanofluidic filter. Anal Chem 77:4293–4299